**International Journal of Environmental and Ecology Research**
**www.environmentaljournal.in**
**Online ISSN: 2664-7117**
**Received: 30-06-2026, Accepted: 30-07-2026, Published: 14-08-2026**
**Volume 8, Issue 3, 2026, Page No. 21-30**

# First geochemical characterization of late Holocene sediments from the Chari River (Lake Chad Basin)

**Jean-Paul Vicat, Jean-Claude Doumnang Mbaigané**
Faculty of Exact and Applied Sciences, Laboratory of Geology, University of N'Djamena, Geomorphology, and Remote Sensing, N'Djamena, Chad
**DOI:** https://doi.org/10.66856/ijeer.2026.8.3.8029

**Abstract**
This study provides the first geochemical characterization of Late Holocene fluvial sediments from the Chari River at N'Djamena. Major, trace, and REE geochemistry was used to investigate the REE resource potential, sediment provenance, weathering intensity, depositional conditions, paleoclimate, and tectonic setting. The clay sample is enriched in most major and trace elements and REE relative to the sandy samples, reflecting grain-size effects and quartz dilution rather than differences in provenance. Total REE concentrations (187–339 ppm) are typical of common siliciclastic sediments, indicating limited potential as a secondary REE resource. Chondrite-normalised REE patterns display moderate LREE enrichment and negative Eu anomalies, indicating derivation from felsic upper continental crust. High CIA, CIW, and PIA values, together with low ICV values and A–CN–K relationships, indicate compositionally mature sediments derived from intensely weathered source rocks. Immobile trace element ratios consistently support a felsic source with a contribution from recycled sedimentary material. Tectonic discrimination diagrams and functions point to an intraplate setting. Multiple redox proxies (U/Th, Ni/Co, and V/Cr) indicate deposition under oxic conditions. The Climatic Index and several geochemical ratios ($K_2O/Al_2O_3$, Mg/Ca, $Al_2O_3$/MgO, Rb/Sr, Ga/Rb, and Sr/Cu) are consistent with deposition under warm and humid climatic conditions.

**Keywords:** Lake Chad Basin, Chari River, Holocene fluvial sediments, geochemistry, REE resource, weathering, provenance, redox conditions, paleoclimate

## Introduction

Sediments are valuable archives of the geological and environmental processes operating within drainage basins and during deposition. Their chemical composition records the combined influence of source-rock lithology, weathering intensity, erosion, transport, hydraulic sorting, and depositional conditions. Major elements, trace elements, and rare earth elements (REE) are widely used as geochemical tracers because they are relatively unaffected by weathering, transport, and diagenesis. Major element compositions and associated weathering indices provide robust constraints on the degree of chemical alteration, sediment recycling, and maturity (Nesbitt and Young, 1982, 1984; Cox *et al*., 1995; Fedo *et al*., 1995) [32, 33, 12, 17]. By contrast, relatively immobile trace elements, including Sc, Ti, V, Cr, Ni, Y, Zr, Nb, Hf, Th, and REE, commonly retain the geochemical fingerprints of their source lithologies (Taylor and McLennan, 1985; Bhatia and Crook, 1986; Cox *et al*., 1995) [44, 7, 12]. Accordingly, the distribution of these elements in sediments has been extensively applied to provenance determination, evaluation of weathering conditions, and identification of the factors controlling sediment composition.

In the Lake Chad Basin, the Chari River is the main tributary of Lake Chad and supplies the bulk of the water and sediment entering the lake. Although the Quaternary deposits associated with the river have been thoroughly investigated from a sedimentological perspective (Moussa, 2010) [31], their geochemical composition remains poorly documented as the few available studies focus on modern river sediments (Digué *et al*., 2023; Wana *et al*., 2024) [14, 51]. A better understanding of the geochemical signature of Holocene sediments is therefore essential to constrain sediment provenance, assess weathering processes within the watershed, and reconstruct paleo-depositional conditions, and establish a natural geochemical baseline against which potential contamination of modern river sediments can be assessed.

This preliminary study presents major, trace, and REE data from four Upper Holocene fluvial sediment samples collected at N'Djaména. The objectives are to (i) provide a first geochemical characterization of these sediments, (ii) evaluate their potential as a secondary resource for REE, (iii) constrain their provenance, (iv) evaluate the degree of chemical weathering in the source areas and the sediment maturity, and (v) assess paleo-depositional conditions.

## Geological Setting

The Lake Chad Basin is extensively covered by Quaternary deposits. Lake Chad is mainly fed by the Chari River and its tributaries (Fig. 1), which form the basin's primary hydrological network. The Chari catchment predominantly drains Quaternary sediments and the Continental Intercalaire, whereas the Precambrian basement is exposed only in the uppermost part of the watershed. The Quaternary deposits consist mainly of unconsolidated sands, silts, and clays derived from fluvial, lacustrine, and aeolian processes. The Continental Intercalaire is composed predominantly of poorly consolidated fluvial and lacustrine sediments, including sandstones, sandy clays, clays, and local ferruginous horizons. The Precambrian basement consists of Proterozoic metamorphic and magmatic rocks belonging to the Pan-African orogenic belt (Bessoles and Trompette, 1980) [5]. It was formed during the collision between the Congo and West African cratons (Castaing *et al*., 1994; Toteu *et al*., 2004) [11, 46] and was stabilized at approximately

600 Ma (Toteu *et al*., 2022) [47]. From N'Djamena to Lake Chad, the Quaternary deposits consist of sediments transported and deposited by the Chari River (Pias, 1967) [34]. From base to top, these units comprise: (i) a succession of light-coloured sands approximately 10 m thick, with variable clay intercalations; (ii) the *Sables Croûtés* (approximately 1 m thick), consisting of darker-coloured sands interbedded with indurated clayey-sand horizons that are resistant to erosion; and (iii) the Upper Grey Series (approximately 1 m thick), which unconformably overlies the underlying unit across an erosional surface and consists of clayey sands that are also resistant to erosion (Moussa, 2010) [31]. Radiocarbon dating of organic matter yielded ages of 1475 ± 30 $^{14}$C yr BP for the upper Upper Grey Series and 3700 ± 40 $^{14}$C yr BP for the basal sands (Moussa, 2010) [31]. These ages place the deposits within the Late Holocene (4.2 ka to present; ICS, 2024) [22]. During this interval, Lake Chad experienced alternating humid and arid phases, along with episodes of significant lake contraction and desiccation (Servant and Servant-Vildary, 1980) [40]. An extensive clay layer in the basal formation is interpreted as a lacustrine deposit associated with the final highstand of the Upper Holocene Mega-Lake Chad (Moussa, 2010) [31].

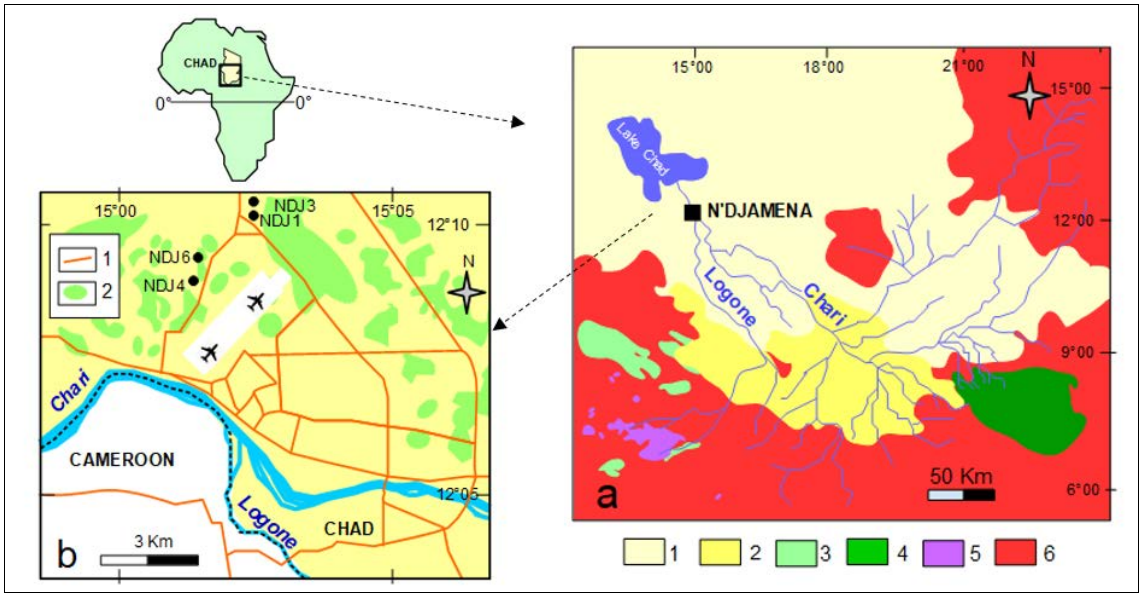


**Fig 1:** (a) Simplified geological map of the Chari River watershed (after Louis, 1970) [26]. 1: Quaternary deposits; 2: Continental Terminal; 3: Middle and Upper Cretaceous; 4: Continental Intercalaire; 5: Cenozoic mafic volcanism of the Cameroon Volcanic Line; 6: Precambrian basement. (b) Location map of the analysed samples. 1: Main roads; 2: Ponds

## Material and Methods

In N'Djamena, a clayey sand sample from the upper part of the Upper Grey Series (NDJ4) was collected at the Goudji quarry (12°09′02.40″N, 15°01′38.62″E), one clay sample from of the basal formation (NDJ6) from the Epervier pond (12°09′21″N, 15°01′43″E), and two sands samples of the basal formation, NDJ1 (12°10′09″N, 15°02′31″E) and NDJ3 (12°10′36″N, 15°02′25″E), from the northern outskirts of the city (Fig. 1b).

Major and trace element analyses were carried out at the *Service d'Analyse des Roches et des Minéraux* (SARM), Nancy, France. Major and trace element concentrations were respectively measured by ICP-OES and ICP-MS. The samples were ground at 70 mm and then approximately 300 mg of powder was prepared by alkaline fusion with $LiBO_2$ at 1000°C and dissolved in 1N $HNO_3$. Calibration and quality control were done with international geostandards (Carigan *et al*., 2001) [10].

## Results and discussion

***Major oxides***. The whole-rock major-element compositions are presented in Table 1. Except for $SiO_2$, the clay sample (NDJ6) exhibits higher concentrations of all other major elements than the clayey sand sample (NDJ4) and the sandy samples (NDJ1 and NDJ3). The PAAS normalised major element patterns (Fig. 2) highlight the compositional contrast between the clay-rich sample and the quartz-rich sandy samples, reflecting the dilution of most major elements by quartz in the latter.

**Table 1:** Major element composition (wt.%) of the studied samples

| | NDJ4 | NDJ6 | NDJ1 | NDJ3 |
|---|---|---|---|---|
| SiO2 | 64.44 | 51.99 | 69.88 | 70.26 |
| TiO2 | 0.93 | 1.17 | 0.89 | 0.81 |
| Al2O3 | 15.87 | 20.36 | 15.97 | 16.89 |
| Fe2O3 | 5.78 | 7.74 | 4.09 | 4.31 |
| MnO | 0.02 | 0.07 | 0.02 | 0.03 |
| MgO | 0.49 | 0.94 | 0.68 | 0.67 |
| CaO | 0.47 | 0.84 | 0.55 | 0.6 |
| Na2O | 0.24 | 0.52 | 0.22 | 0.17 |
| K2O | 1.45 | 1.80 | 1.28 | 1.12 |
| P2O5 | 0.11 | 0.18 | 0.13 | 0.21 |
| Pf | 10.06 | 14.28 | 4.6 | 4.79 |
| Total | 89.80 | 85.61 | 93.71 | 95.07 |
| ICV | 0.56 | 0.65 | 0.51 | 0.48 |
| CIA | 87 | 85 | 88 | 91 |
| PIA | 95 | 91 | 95 | 97 |
| CIW | 95 | 92 | 96 | 97 |
| K2O/Al2O3 | 0.09 | 0.09 | 0.08 | 0.07 |
| Al2O3/MgO | 32 | 22 | 23 | 25 |
| Mg/Ca | 0.9 | 0.9 | 1.0 | 0.9 |

Geochemical indices and ratios were calculated using anhydrous major element concentrations

ICV = ($Fe_2O_3$+$K_2O$+$Na_2O$+CaO+MgO+$TiO_2$) / $Al_2O_3$ from Cox *et al*. (1995) [12]

CIA (%) = [$Al_2O_3$ / ($Al_2O_3$+CaO*+$Na_2O$+$K_2O$] x 100 from Nesbitt and Young (1984) [33]
PIA (%) = [($Al_2O_3$-$K_2O$) / ($Al_2O_3$+CaO*+$Na_2O$–$K_2O$)] x 100 from Fedo *et al.* (1995) [17]
CIW = [$Al_2O_3$ / ($Al_2O_3$+CaO*+$K_20$)] x 100 from Nesbitt and Young (1982) [32]
CaO*= CaO-$P_2O_5$ x (10/3); if CaO* > $Na_2O$ then CaO*= $Na_2O$

NDJ6, the clay sample, displays relative enrichments in $TiO_2$, $Al_2O_3$, $Fe_2O_3$, and $P_2O_5$ compared to PAAS, reflecting the concentration of clay minerals and relatively immobile phases during weathering. In contrast, MnO, MgO, CaO, $Na_2O$, and $K_2O$ are markedly depleted relative to PAAS. The depletion in CaO and $Na_2O$ indicates alteration and destruction of plagioclase feldspars, whereas the low MgO contents suggest the removal of ferromagnesian minerals during chemical weathering. The depletion in $K_2O$ reflect intense leaching of mobile alkali elements and the destruction of K-feldspar and mica. The negative MnO anomaly probably results from the high mobility of Mn under fluctuating redox conditions, leading to its dissolution and removal during weathering. Overall the NDJ6 profile is consistent with an intensely weathered clay-rich sediment depleted in mobile elements but relatively enriched in immobile aluminosilicate and Fe–Ti-bearing phases.

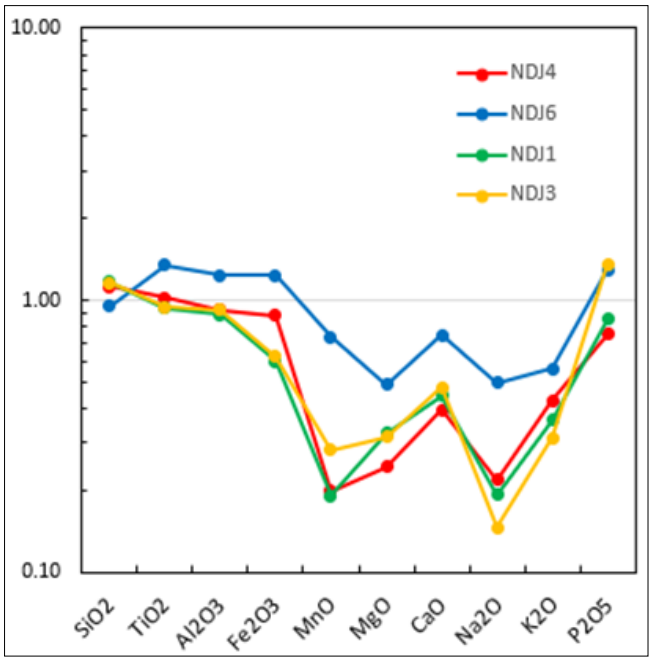


**Fig 2:** Anhydrous recalculated major element concentrations normalised to PAAS (after Pourmand *et al.*, 2012) [34]

The clayey sand sample (NDJ4) and the sandy samples (NDJ1 and NDJ3) exhibit similar PAAS normalised pattern characterized by a slight enrichment in $SiO_2$ and nearly identical $Al_2O_3$, $TiO_2$ values relative to PAAS. In contrast, $Fe_2O_3$ and MnO are slightly depleted, whereas MgO, CaO, $Na_2O$, and $K_2O$ display marked negative anomalies. The relative enrichment in $SiO_2$ reflects an increased proportion of quartz compared to PAAS, consistent with the more sandy character of the sediment. The near-flat $TiO_2$ pattern suggests that Ti-bearing resistant minerals remained relatively preserved during sedimentary processes and weathering. The depletion in $Fe_2O_3$ and MnO may indicate partial loss of Fe–Mn bearing phases during weathering or hydraulic sorting. The strong depletion in MgO, CaO, and $Na_2O$ reflects extensive alteration and removal of unstable ferromagnesian minerals and plagioclase feldspars, whereas the low $K_2O$ contents suggest depletion in K-feldspar and micas. Overall, the profiles indicate mature sediment affected intense chemical weathering and the removal of feldspars, ferromagnesian minerals, aluminosilicate fraction, and quartz enrichment. The positive $P_2O_5$ anomaly in NDJ6 and NDJ3 may be attributed to the presence of apatite, adsorption onto clay minerals, or localized organic and/or phosphatic inputs.

**REE:** The results of REE analysed are shown in Table 2. The total REE content is high (187–339 ppm). The ratios of LREE/HREE (7.75–10.61; Table 2) are comparable to those of UCC (9.34; Rudnick and Gao, 2014) [39] and PAAS (9.52; Taylor and McLennan, 1985) [44]. REE concentrations are higher in the clay sample (NDJ6; 339 ppm; Table 2) than in the clayey sand sample (NDJ4; 266 ppm; Table 2) and in the sandy samples (187–218 ppm; Table 2). This difference is mainly due to quartz dilution in the sandy samples and to the preferential association of REE with fine-grained mineral phases, such as clays and Fe-Mn oxyhydroxides, present in NDJ6.

**Table 2:** REE concentrations (ppm) and their calculated ratios

| | NDJ4 | NDJ6 | NDJ1 | NDJ3 |
|---|---|---|---|---|
| La | 59.62 | 77.13 | 40.33 | 45.13 |
| Ce | 109.65 | 138.52 | 76.03 | 94.33 |
| Pr | 13.08 | 17.20 | 8.97 | 10.33 |
| Nd | 47.98 | 62.69 | 32.53 | 39.37 |
| Sm | 9.33 | 11.63 | 6.58 | 7.04 |
| Eu | 1.91 | 2.42 | 1.24 | 1.38 |
| Gd | 7.36 | 9.11 | 5.76 | 5.61 |
| Tb | 1.17 | 1.39 | 0.93 | 0.94 |
| Dy | 6.25 | 7.78 | 5.58 | 5.31 |
| Ho | 1.30 | 1.47 | 1.21 | 1.03 |
| Er | 3.45 | 4.15 | 3.37 | 3.02 |
| Tm | 0.53 | 0.65 | 0.55 | 0.46 |
| Yb | 3.55 | 3.99 | 3.52 | 3.27 |
| Lu | 0.48 | 0.63 | 0.48 | 0.47 |
| SREE | 265.66 | 338.76 | 187.08 | 217.69 |
| SLREE/SHREE | 10.03 | 10.61 | 7.75 | 9.83 |
| $La/Yb_{NC}$ | 11.41 | 13.13 | 7.78 | 9.38 |
| $La/Yb_{NPAAS}$ | 1.14 | 1.31 | 0.77 | 0.93 |
| $Eu/Eu^*_{NC}$ | 0.70 | 0.72 | 0.61 | 0.67 |
| $Eu/Eu^*_{NPAAS}$ | 1.22 | 1.25 | 1.07 | 1.17 |
| $Ce/Ce^*_{NPAAS}$ | 0.95 | 0.92 | 0.97 | 1.05 |
| $Pr/Pr^*_{NPAAS}$ | 1.02 | 1.04 | 1.02 | 0.96 |

$(La/Yb)_{NC} = (La_{sample}/La_{chondrite}) / (Yb_{sample}/Yb_{chondrite})$
$(La/Yb)_{NPAAS} = (La_{sample}/La_{PAAS}) / (Ybsample/Yb_{PAAS})$
$Eu/Eu^*_{NC} = (Eu_{sample}/Eu_{chondrite}) / [(Sm_{sample}/Sm_{chondrite}) \times (Gd_{sample}/Gd_{chondrite})]^{1/2}$
$Eu/Eu^*_{NPAAS} = (Eu_{sample}/Eu_{PAAS}) / [(Sm_{sample}/Sm_{PAAS}) \times (Gd_{sample}/Gd_{PAAS})]^{1/2}$
$Ce/Ce^*_{NPAAS} = (Ce_{sample}/Ce_{PAAS}) / [(La_{sample}/La_{PAAS}) \times (Pr_{sample}/Pr_{PAAS})]^{1/2}$
$Pr/Pr^*_{NPAAS} = (Pr_{sample}/Pr_{PAAS}) / [(Ce_{sample}/Ce_{PAAS}) \times (Nd_{sample}/Nd_{PAAS})]^{1/2}$
$Eu/Eu^*_{NPAAS} = (Eu_{sample}/Eu_{PAAS}) / [(Sm_{sample}/Sm_{PAAS}) \times (Gd_{sample}/Gd_{PAAS})]^{1/2}$

Chondrite normalised patterns calculated after Mc Dounough and Sun (1995) [28] display subparallel patterns (Fig. 3). They show moderate light rare earth element (LREE) enrichment relative to heavy rare earth elements (HREE), with $La/Yb_{NC}$ ratios of 7.78–13.13 (Table 2)

indicating a slight preferential enrichment of LREE in the clay sample. The samples display a negative europium anomaly ($Eu/Eu^*_{NC}$ = 0.61–0.72; Table 2) reflecting plagioclase fractionation during source rock evolution.

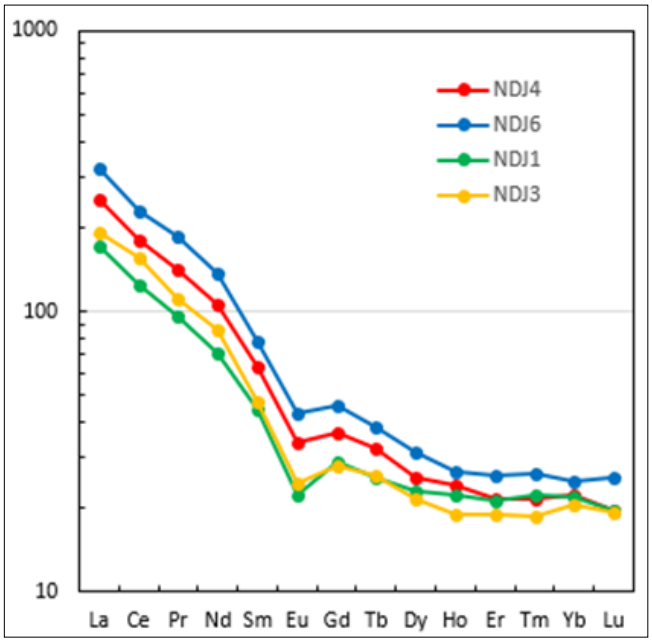


**Fig 3:** REE patterns normalised to chondrite from Mc Dounough and Sun (1995) [28]

PAAS normalised patterns (Fig. 4) calculated after Pourmand *et al.* (2012) [35] yield relatively low $(La/Yb)_{NPAAS}$ values (0.77–1.31; Table 2), indicating only modest LREE depletion or enrichment compared to PAAS. The subparallel REE patterns, combined with enrichment in the clay sample, indicates that grain-size sorting exerts a primary control on REE distribution, while provenance remains unchanged between the two lithologies. The europium anomaly is slightly positive ($Eu/Eu^*_{NPAAS}$ = 1.07–1.25; Table 2), indicating that the studied sediments are less depleted in Eu than PAAS.

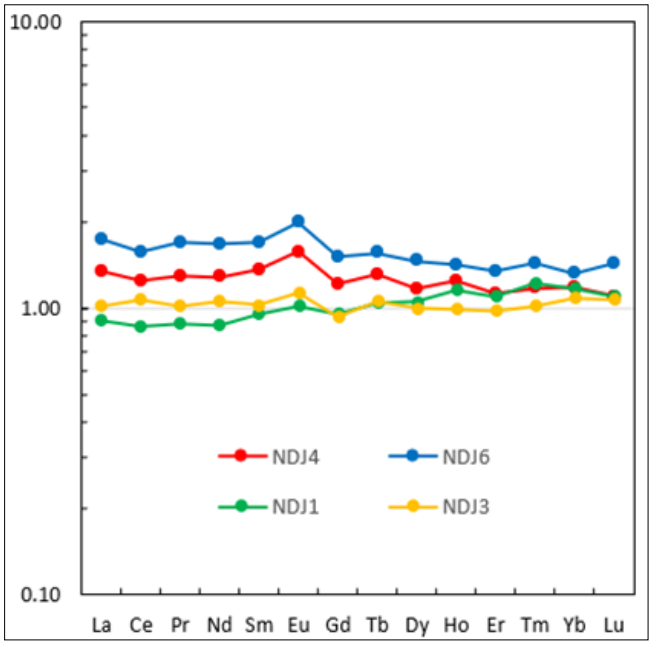


**Fig 4:** REE patterns normalised to PAAS from Pourmand *et al.* (2012) [35]

In recent years, sediments have emerged as a promising secondary resource for REE, providing an alternative to conventional REE-bearing ores (Dushyantha *et al.*, 2021; Batapola *et al.*, 2023; Xu *et al.*, 2025) [16, 2, 55]. The REE concentrations (ΣREE = 187–339 ppm; Table 2) of our samples are typical of siliciclastic sediments and are substantially lower than those reported for potentially exploitable REE deposits, such as the clays of southern China (1,000–3,000 ppm; Xie *et al.*, 2016) [52], or deep-sea sediments from the Pacific Ocean (2,000–5,000 ppm; Kato *et al.*, 2011) [24]. These concentrations are also lower than those reported for sediments from the Mugheb Basin within the Cameroon Volcanic Line (215–458 ppm), which have been identified as a potential future source of REE (Yika *et al.*, 2026) [56]. Therefore, the studied sediments do not appear to constitute a promising secondary REE resource.

**Trace elements:** The results of trace elements analysed are shown in Table 3. The spider plot of trace elements normalised to PAAS after Taylor and McLennan (1985) [44] (Fig.5) are globally close to the PAAS values.

**Table 3:** Trace elements concentration (ppm) and their calculated ratios

| | NDJ4 | NDJ6 | NDJ1 | NDJ3 |
|---|---|---|---|---|
| Be | 2.61 | 3.75 | 2 | 1.81 |
| V | 100.67 | 109.78 | 63.86 | 64.61 |
| Cr | 80.43 | 104.99 | 62.61 | 61.88 |
| Co | 10.31 | 17.56 | 9.2 | 11.18 |
| Ni | 33.08 | 48.83 | 25.19 | 25.79 |
| Cu | 31.82 | 40.18 | 26.6 | 29.79 |
| Ga | 22.99 | 30.28 | 16.83 | 17.32 |
| Ge | 1.89 | 1.92 | 1.28 | 1.36 |
| Rb | 89.99 | 121.40 | 87.66 | 92.05 |
| Sr | 75.64 | 122.88 | 102.68 | 107.6 |
| Y | 37.11 | 43.57 | 35.91 | 31.66 |
| Zr | 322.08 | 341.28 | 408.21 | 447.6 |
| Nb | 27.88 | 34.24 | 20.03 | 21.56 |
| Mo | 1.01 | 1.37 | 0.89 | 1.09 |
| Cs | 4.17 | 5.50 | 2.92 | 3.22 |
| Ba | 502.29 | 629.19 | 585.07 | 600.3 |
| Hf | 7.85 | 8.84 | 10.06 | 10.8 |
| Ta | 2.40 | 2.84 | 1.74 | 1.78 |
| W | 1.43 | 1.95 | 1.32 | 1.4 |
| Bi | 0.31 | 0.37 | 0.26 | 0.23 |
| Th | 20.97 | 25.30 | 15.96 | 16.65 |
| U | 5.41 | 6.89 | 4.15 | 4.00 |
| U/Th | 0.26 | 0.27 | 0.26 | 0.24 |
| Ni/Co | 3.21 | 2.78 | 2.74 | 2.31 |
| V/Cr | 1.25 | 1.05 | 1.02 | 1.04 |
| Rb/Sr | 1.19 | 0.99 | 0.85 | 0.86 |

Except for Zr and Hf trace elements are mostly enriched in the clay sample (NDJ6) relative to the other samples. The relatively higher abundances of Zr and Hf in the sandy samples likely result from hydraulic sorting, which concentrates dense heavy minerals in the coarser sediment fraction, whereas most other trace elements are

preferentially associated with clay minerals and Fe–Mn oxyhydroxides.

V, Cr, Ni, Co, Cu and W are only slightly depleted relative to PAAS in the clay sample (NDJ6) but are more strongly depleted in the other samples. This systematic pattern indicates a dominant grain-size control. These elements are preferentially concentrated in the fine fraction through their association with clay minerals and/or Fe–Mn oxyhydroxides, whereas quartz-rich sandy sediments dilute their concentrations. For V, Cr, Ni, Co and Cu, the generally low abundances also suggest a limited contribution from mafic minerals in the source area.

Rb, Sr and Cs are depleted in the four samples. This depletion most likely reflects the relatively low abundance of feldspars and K-bearing minerals in the Chari sediments. Strontium is mainly hosted by plagioclase, whereas Rb and Ce preferentially substitute for K in K-feldspars and micas. Their depletion is therefore consistent with quartz-rich and compositionally mature nature of sediments.

Th and U are slightly enriched relative to PAAS and display higher concentrations in the clay sample (NDJ6) than in the other samples. This pattern is mainly controlled by grain size. Thorium is primarily hosted by Th-bearing accessory minerals, such as monazite and allanite, which commonly occur as very fine grains and are preferentially concentrated in the silt and clay fractions rather than in quartz-rich sands. Uranium is mainly associated with clay minerals and Fe–Mn oxyhydroxides. Consequently, the enrichment of both elements in NDJ6 reflects the concentration of fine-grained mineral phases, whereas their lower abundances in the sandy samples mainly result from dilution by quartz.

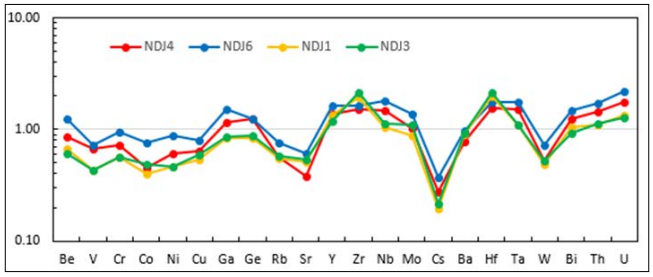


**Fig 5:** Spider plot of trace elements normalised to PAAS (Taylor and McLennan, 1985) [44]

**Sediment Maturity and Weathering**

The Index of Compositional Variability (ICV) introduced by Cox al. (1995) [12] is used to assess sediment maturity. Sediments with ICV > 1 are considered immature, whereas those with ICV < 1 are regarded as mature. The relationship between the Chemical Index of Alteration (CIA) proposed by Nesbitt and Young (1982) [32] and the ICV is commonly used to evaluate the combined effects of chemical weathering and sediment recycling (Guo *et al.*, 2024; Togozo *et al.*, 2025) [20, 45]. In the present study, the ICV–CIA relationships indicate that all four samples plot within a compositional domain indicative of mature and strongly weathered materials (Fig. 6). Low ICV values (0.51–0.65; Table 1) suggest compositionally mature sediments, consistent with prolonged chemical weathering and/or sediment recycling. High CIA values (85–91; Table 1) further indicate intense chemical weathering in the source area or during sediment recycling, likely under warm and humid climatic conditions.

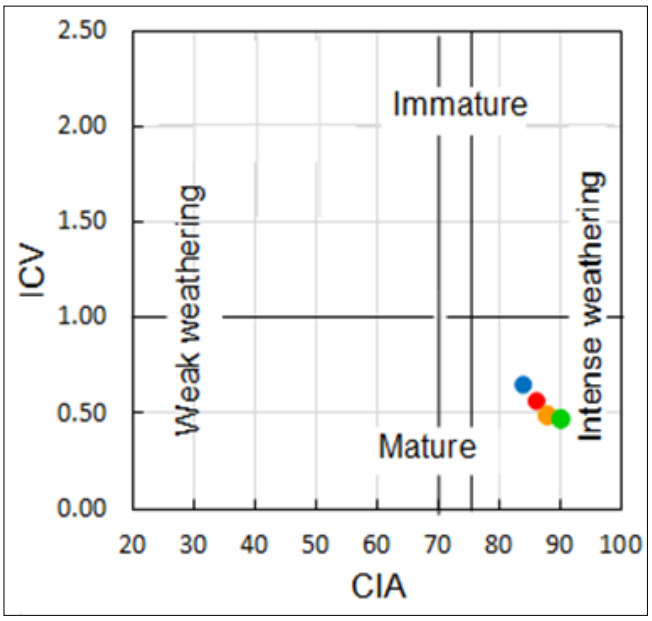


**Fig 6:** ICV vs CIA diagram. Same legend as in Fig. 5

The limited variation among samples suggests derivation from a broadly homogeneous, pre-weathered source. However, the slightly higher ICV value in the clay sample (NDJ6), together with a marginally lower CIA, may reflect subtle mineralogical differences, possibly related to a relative enrichment in Fe-bearing phases or accessory minerals, rather than a decrease in the overall degree of chemical weathering. Overall, the ICV–CIA systematics suggest that sediment composition is largely inherited from pre-weathered source materials and subsequently modified by grain-size sorting and minor mineralogical fractionation, rather than by significant variations in weathering intensity.

The Plagioclase Index of Alteration (PIA) proposed by Fedo *et al.* (1995) [17] is very high (91–97%; Table 1), indicating almost complete destruction of plagioclase during chemical weathering. Similarly, the Chemical Index of Weathering (CIW) of Nesbitt and Young (1982) [32] is also very high (92–97%; Table 1), confirming an extreme degree of chemical alteration.

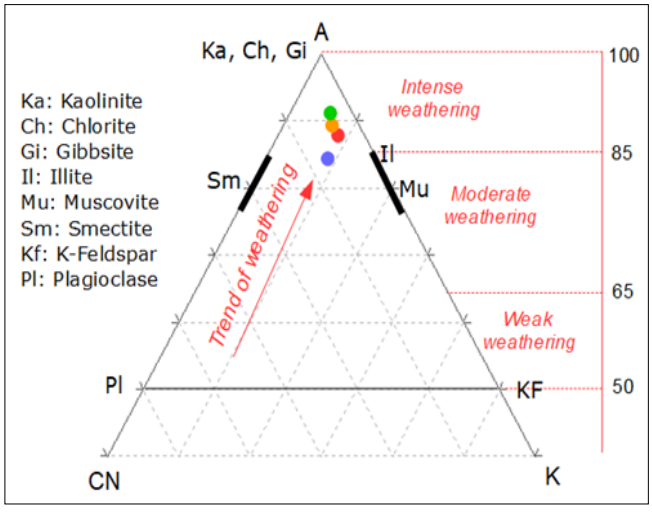


**Fig 7:** A–CN–K ternary diagram (Nesbitt and Young, 1984) [32]. Same legend as in Fig. 5

In the A–CN–K diagram (Nesbitt and Young, 1984) [32] (Fig. 7), the samples plot close to the $Al_2O_3$ apex, with high A values (84.8–90.5%) and low CN contents (3.0–7.1%). This marked depletion of Ca and Na reflects intense plagioclase alteration, consistent with warm and humid climatic conditions that promote strong hydrolytic weathering. The samples follow the typical weathering trend toward the aluminous clay mineral field, which aligns with the high CIA, CIW, and PIA values. Overall, the diagram indicates chemically mature sediments derived from strongly weathered source rocks.

**Provenance**

The Roser and Korsch (1988) [37] diagram (Fig. 8) classically used for provenance determination, places samples NDJ1 and NDJ3 in the field of quartzose sediments of mature continental provenance, and NDJ4 and NDJ6 in the mafic field. This contradicts the nature of the Chari catchment, which is predominantly composed of felsic rocks. This discrepancy reflects the limitation of this diagram for highly weathered mature sediments for which the leaching of the most mobile major elements (Ca, Na, K) leads to erroneous results (Cox *et al*., 1995) [12].

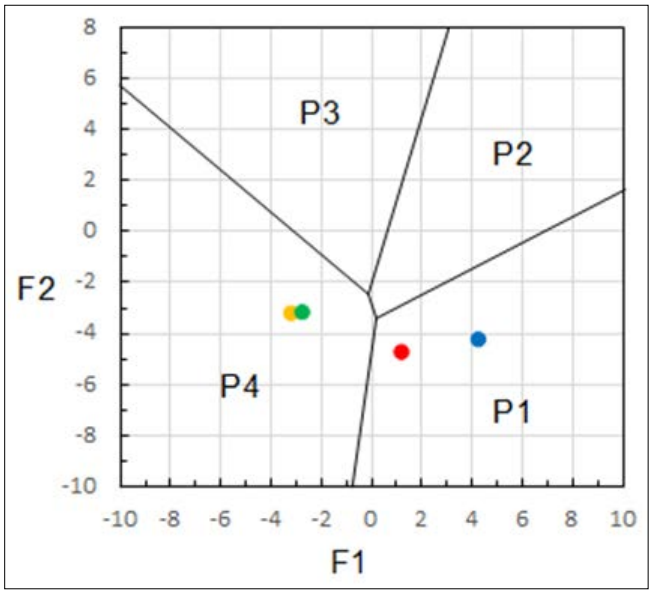


**Fig 8:** Roser and Korsch (1988) [37] diagram. P1: mafic igneous provenance. P2: intermediate igneous provenance. P3: felsic igneous provenance. P4: quartzose sediments of mature continental provenance. Same legend as in Fig. 5

The diagrams (not shown) based on relatively immobile elements, such as Cr vs. Ni (Garver *et al*., 1996) [19], Cr/V vs. Y/Ni (McLennan *et al*., 1993) [30], $TiO_2$ vs. Zr (Hayashi *et al*., 1997) [21], and the Ni–V–Th*10 diagram (Bracciali *et al*., 2007) [8] indicate a felsic source without significant mafic input, which is consistent with the predominantly felsic composition of the Chari catchment.

The negative Eu anomaly observed in the REE/chondrite patterns (Fig. 3), the $La/Yb_{NC}$, and the LREE/HREE ratios (Table 1) also suggests derivation from felsic upper continental crust sources (Taylor and McLennan, 1985) [44]. More precisely, the positive Eu anomaly in the REE/PAAS patterns (Fig. 4) is consistent with observations from most large river sediments worldwide (Bayon *et al*., 2015) [4], whose catchments have diverse lithologies, such in the Chari Basin (Fig. 1), rather than a strictly granitic source, which would typically display a negative Eu anomaly (Singh, 2009) [42].

The La/Th vs. Hf diagram (Floyd and Leveridge, 1987) [18], initially developed for discriminating the tectonic settings of source rocks associated with island arcs but subsequently applied to provenance analysis of siliciclastic sedimentary rocks, furthermore indicates a significant contribution from recycled older sedimentary material (Fig. 9).

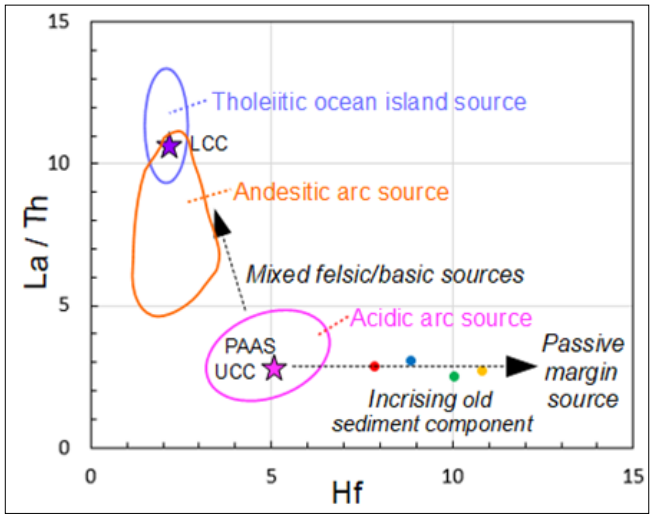


**Fig 9:** La/Th vs Hf diagram (after Floyd and Leveridge, 1987) [18]. UCC, Upper continental Crust and LCC, Lower Continental Crust after Taylor and MC Lennan (1985) [44]. Same legend as in Fig. 5

**Tectonic Setting**

The tectonic discrimination diagram of Bhatia (1983) [6] (not shown) place the samples in the passive margin field. The tectonic discrimination diagram of Verma and Armstrong-Altrin (2013) [49] (not shown) indicate a continental rift, while the $DF_{(A–P)M}$ (−2.26 to −1.29) and $DF_{(A–P)MT}$ (2.44 to 4.51) values obtained using the discriminant functions of Verma and Armstrong-Altrin (2016) [50] indicate a passive margin setting (Fig. 10). Together, these results consistently indicate an intraplate tectonic environment. The Chari sediments are derived predominantly from the recycling of Quaternary deposits and the Continental Terminal Formation, with a lesser contribution from the Pan-African basement. Consequently, the inferred intraplate affinity reflects the mature composition of recycled sediments, thereby overprinting the primary tectonic signature of the Pan-African basement.

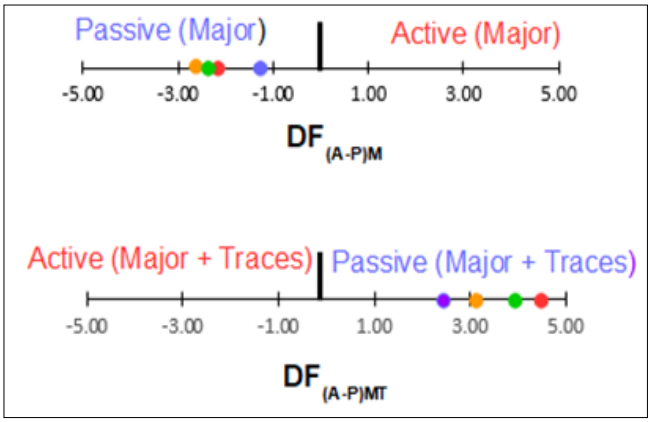


**Fig 10:** Discriminant functions (DF) after Verma and Armstrong-Altrin (2016). Same legend as in Fig. 5

**Redox conditions**

Redox conditions strongly control trace element mobility and enrichment during sediment deposition by regulating their oxidation state, solubility, and fixation in mineral phases. The Ce anomaly $Ce/Ce^*_{NPAAS}$ is commonly used as a redox proxy because Ce is the only REE that can be significantly oxidized from $Ce^{3+}$ to the less soluble $Ce^{4+}$ under oxidizing conditions, leading to its preferential removal from solution and the development of negative Ce anomalies. In contrast, reducing conditions generally inhibit this process and may preserve or even produce positive Ce anomalies. The Ce anomalies observed in the studied samples are weak (0.92–1.05; Table 2). According to the Ce/Ce* vs. Pr/Pr* discrimination approach proposed by Bau and Dulski (1996) [3] (Fig. 11), with $Pr/Pr^*_{NPAAS}$ values varying between 0.96 and 1.04 (Table 2), the observed Ce anomalies are apparent, and reflect minor anomalies in La rather than significant redox-controlled Ce fractionation.

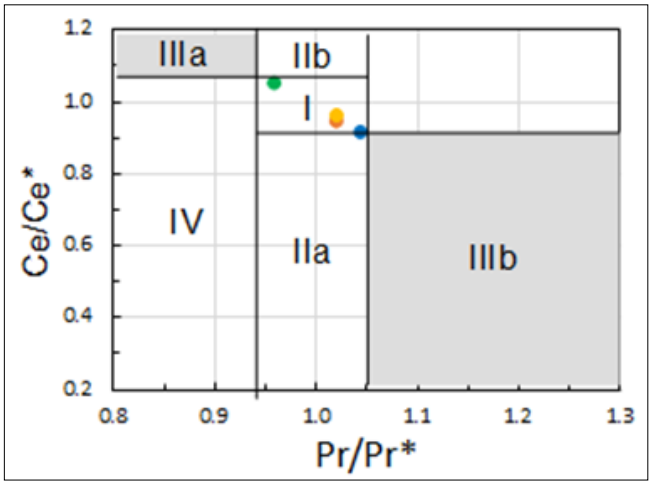


**Fig 11:** $(Pr/Pr^*)_{NPAAS}$ versus $(Ce/Ce^*)_{NPAAS}$ diagram (after Bau and Dulski, 1996) [3]. I: neither Ce no La anomaly; IIa: positive La anomaly, no Ce anomaly; IIb : negative La anomaly, no Ce anomaly; IIIa: positive Ce anomaly; IIIb: negative Ce anomaly. Same legend as in Fig. 5

Several relatively immobile trace-element ratios are commonly used to assess redox conditions in sedimentary depositional environments (reviewed in Tribovillard *et al*., 2006) [48]. The U/Th ratio is a widely used proxy: low values (< 0.75) indicate oxic conditions, whereas high values (> 1.25) reflect anoxic settings (Jones and Manning, 1994) [23]. The studied samples display low U/Th ratios (0.24–0.27; Table 3), pointing to deposition under oxic conditions. Similarly, Ni/Co ratios < 5 are indicative of oxic conditions, whereas values > 5 suggest suboxic to anoxic environments (Jones and Manning, 1994; Madhavaraju *et al*., 2016) [23, 27]. The low Ni/Co ratios obtained here (2.31–3.21; Table 3) support deposition under oxic conditions. Similarly, V/Cr ratios below 2 (1.02–1.25; Table 3) are also indicative of an oxic depositional environment (Rimmer, 2004) [36].

**Climate**

The high CIA, CIW, and PIA values, together with the sample positions in the A–CN–K diagram of Nesbitt and Young (1984) [33], point to a warm and humid climate. Several major and trace element ratios are also commonly used as geochemical proxies to reconstruct the paleoclimatic conditions that prevailed during sediment deposition (reviewed in Shaltami and Ben Hkoma, 2024) [41].

Humid climatic conditions are typically associated with low $K_2O/Al_2O_3$ ratios (<0.2), whereas values >0.2 are indicative of arid environments (Roy and Roser, 2013) [38]. The consistently low $K_2O/Al_2O_3$ ratios (0.07–0.09; Table 1) obtained for the studied samples therefore support deposition under a humid climatic regime.

The Mg/Ca ratio is highly sensitive to climatic shifts. In general, high ratios indicate aridity, whereas low ratios reflect humid conditions (Song, 2005) [43]. The low Mg/Ca values of the studied samples (0.9–1.0; Table 1) are consistent with a humid climate.

Similarly, the $Al_2O_3$/MgO ratio in clay minerals serves as a useful paleoclimatic indicator, with high values reflecting warm-humid conditions and low values indicating drier climates (Liu and Zhou, 2007) [25]. The elevated $Al_2O_3$/MgO ratios obtained here (22–32; Table 1) further support warm and humid climatic conditions.

The Rb/Sr ratio is a widely used geochemical proxy for evaluating paleoweathering intensity and associated paleoclimatic conditions in sedimentary rocks (Zou *et al*., 2021) [57]. During chemical weathering, Sr primarily hosted in plagioclase and carbonates, is readily mobilized and removed by leaching, whereas Rb, commonly associated with K-bearing clay minerals and micas, tends to be retained in the weathering products (Nesbitt and Young, 1982; Cox *et al*., 1995) [32, 12]. Consequently, increasing Rb/Sr ratios generally reflect progressive depletion of mobile cations under intensified chemical weathering in warm and humid climates. Low Rb/Sr values (<5) are typically associated with weak weathering and relatively arid or cold conditions, whereas moderate to high values (>5) indicate stronger hydrolytic alteration and enhanced leaching (Cullers, 2000; Zou *et al*., 2021) [13, 57] . However, this ratio may also be influenced by sediment recycling, grain-size sorting, mineralogical composition, and quartz dilution, particularly in compositionally mature sediments (Cox *et al*., 1995) [12]; it is therefore most reliably interpreted in combination with major-element weathering indices such as CIA. In the present study, the high CIA values (81–86; Table 1), together with moderate Rb/Sr ratios (0.85–1.19; Table 3), further corroborate intense chemical weathering of the source rocks under warm and humid climatic conditions

The Climatic Index (C.I.) is also used to characterize the paleoclimate. Under humid climatic conditions, intense chemical weathering promotes the leaching of soluble cations, whereas relatively immobile elements such as Fe, Mn, Cr, Ni, V, and Co are preferentially retained in soils and sediments through their association with clay minerals and Fe–Mn oxyhydroxides. Conversely, under arid conditions, limited chemical weathering and intense evaporation favour the accumulation of relatively mobile elements such as Ca, Mg, Na, K, Sr, and, to a lesser extent, Ba through the precipitation of carbonate and evaporite minerals. Based on these contrasting geochemical behaviours, the Climatic Index calculated as C.I. = (Fe + Mn + Cr + Ni + V + Co) / (Ca + Mg + Sr + Ba + K + Na) (Cao *et al*., 2012) [9], has been proposed as a proxy for paleoclimatic conditions. According to the classification established by Ding *et al*. (2018) [15] and Awan *et al*. (2020) [1], C.I. values > 0.8 indicate humid climates, whereas values of 0.6–0.8, 0.4–0.6, 0.2–0.4, and < 0.2 correspond to semi-humid, semi-humid to semi-arid, semi-arid, and arid

climates, respectively. Although grain-size sorting and source-rock composition may also influence the C.I., the consistently high values obtained for all samples (1.2–2.2) are consistent with deposition under a humid climatic regime.

The Ga/Rb versus Sr/Cu diagram provides complementary information on the intensity of chemical weathering and paleoclimatic conditions (Xie *et al*., 2018) [53]. The Ga/Rb ratio is widely used as an indicator of the intensity of hydrolytic weathering. Gallium is relatively immobile and becomes concentrated in Al-rich secondary minerals, especially kaolinite, during weathering (Nesbitt and Young, 1982; McLennan, 1993). By contrast, Rb, which is mainly hosted in K-feldspar and micas, is released during their alteration. Although some Rb is incorporated into illite, much of it is removed by leaching as chemical weathering intensifies. As a result, higher Ga/Rb ratios are characteristic of stronger weathering under warm and humid climatic conditions. In contrast, Sr is preferentially enriched under arid conditions because evaporation promotes its incorporation into carbonate and evaporite minerals, whereas Cu is mainly associated with organic matter and tends to be preserved in sediments deposited under humid conditions. Consequently, Sr/Cu values lower than approximately 5 generally indicate humid climatic conditions, whereas values above 5 indicate cool and/or arid climates (Xu *et al*., 2017) [53].

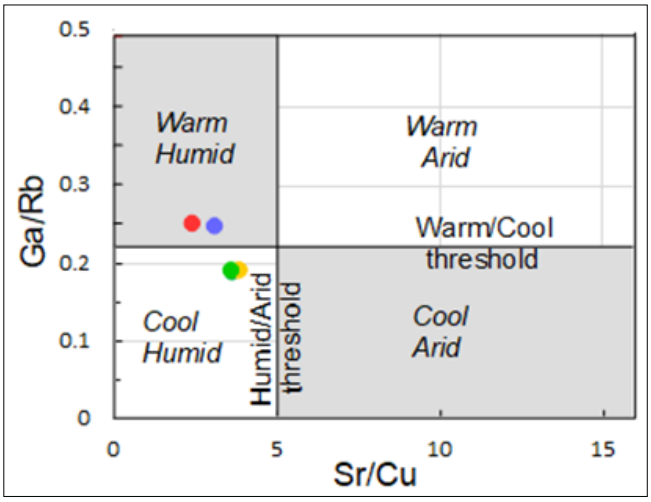


**Fig 12:** Ga/Rb versus Sr/Cu diagram (after Xie *et al*., 2018) [53]. Same legend as in Fig. 5

In the Ga/Rb versus Sr/Cu diagram of Xie *et al*. (2018) [53] (Fig. 12), the clay (NDJ6) and clayey sand (NDJ4) samples indicate a warm and humid climate. The slightly lower Ga/Rb values of the quartz-rich sandy samples (NDJ1 and NDJ3) are interpreted as the result of grain-size sorting and quartz dilution rather than cooler climatic conditions during the Upper Holocene. Overall, the geochemical data consistently support a warm and humid paleoclimate.

## Conclusion

The geochemical signatures of the studied sediments indicate that their composition is predominantly governed by the interplay of intense chemical weathering, sediment recycling, and grain-size sorting. The combined use of major elements, immobile trace elements, REE, and weathering indices enables a coherent reconstruction of the Late Holocene sedimentary system of the Chari River, indicating derivation from predominantly felsic source rocks, with deposition occurring under oxic conditions in a warm, humid climate. The low REE concentrations preclude any significant economic potential. This study provides the first geochemical baseline for Holocene Chari River sediments. Despite being limited to four samples, these findings establish a valuable foundation for future research on paleoenvironmental reconstructions and environmental geochemistry in the Lake Chad basin.

## References


1. Awan RS, Liu C, Gong H, Dun C, Tong C, Chamssidini LG. Paleo-sedimentary environment in relation to enrichment of organic matter of Early Cambrian black rocks of Niutitang Formation from Xiangxi area China. Marine and Petroleum Geology,2020:112:104057.
2. Batapola N, Ratnayake N, Abeysinghe B, Premasiri R, Dushyantha N, Ilankoon IMSK, et al. The potential of REEs in the Eppawala Phosphate Deposit, Sri Lanka: REE enrichment, mineralization, and economic significance. Environ Earth Sci,2023:82(19):446.
3. Bau M, Dulski P. Distribution of Yttrium and Rare-Earth Elements in the Penge and Kuruman Iron-Formations, Transvaal Supergroup, South Africa. Precambrian Research,1996:79:37–55.
4. Bayon GS, Toucanne S, Skonieczny C, André L, Bermell S, Cheron S, et al. Rare earth elements and neodymium isotopes in world river sediments revisited. Geochimica et Cosmochimica Acta,2015:170:17–38.
5. Bessoles B, Trompette R. Géologie de l'Afrique : La chaine panafricaine, zone mobile d'Afrique Centrale (partie Sud) et zone soudanaise. Mémoire BRGM, 1980, 92.
6. Bhatia MR. Plate Tectonics and Geochemical Composition of Sandstone. The Journal of Geology,1983:91:611–627.
7. Bhatia MR, Crook KAW. Trace element characteristics of greywacke and tectonic setting discrimination of sedimentary basins. Contrib Mineral Petrol,1986:92:181–93.
8. Bracciali L, Marroni M, Pandolfi L, Rocchi S. Geochemistry and petrography of Western Tethys Cretaceous sedimentary covers: Implications for provenance and source-rock composition. Geological Magazine,2007:144(1):75–94.
9. Cao J, Wu M, Chen Y, Hu K, Bian L, Wang L, et al. Trace and rare earth element geochemistry of Jurassic mudstones in the northern Qaidam Basin, northwest China. Geochemistry, 1,2012:72(3):245–252.
10. Carignan J, Hild P, Mevelle G, Morel J, Yeghicheyan D. Routine analyses of 551 trace elements in geological samples using flow injection and low-pressure on-line liquid 552 chromatography coupled to ICP-MS: a study of reference materials BR, DR-N, UB-N, AN-G553, and GH. Geostandards and Geoanalytical Research,2001:25:187–198.
11. Castaing C, Feybesse JL, Thiéblemont D, Triboulet C, Chevremont P. Paleographical reconstruction of the Pan-African / Brasiliano orogen: closure of an oceanic domain or intracontinental convergence between major blocks. Precambrian Research,1994:69:327–344.
12. Cox R, Lowe DR, Cullers RL. The influence of sediment recycling and basement composition on

evolution of mudrock chemistry in the southwestern United States. Geochem. Cosmochim. Acta,1995:59(14):2919e2940.
13. Cullers RL. The Geochemistry of Shales, Siltstones and Sandstones of Pennsylvanian-Permian Age, Colorado, USA: Implications for Provenance and Metamorphic Studies. Lithos,2000:51:181–203.
14. Digué TM, Tinda D, Bertrand NG, Salomon MB, Dikdim DJM, Mianpereum T. Contamination and Potential Risks of Heavy Metals in the Sediments of the Chari and Logon Rivers in N'Djamena, Chad. Open Journal of Soil Science,2023:13:29–45.
15. Ding J, Zhang J, Tang X, Huo Z, Han S, Lang Y, et al. Elemental geochemical evidence for depositional conditions and organic matter enrichment of black rock series strata in an inter-platform basin: The Lower Carboniferous Datang Formation, Southern Guizhou, Southwest China. Minerals,2018:8(11):509.
16. Dushyantha NP, Ratnayake NP, Premasiri HMR, Ilankoon IMSK, Hemalal PVA, Jayawardena CL, et al. Leaching of Rare Earth Elements (REEs) from lake sediments around Eppawala phosphate deposit, Sri Lanka: A secondary source for REEs. Hydrometallurgy,2021:205:105751.
17. Fedo CM, Nesbitt HW, Young GM. Unraveling the effects of potassium metasomatism in sedimentary rocks and paleosols, with implications for paleoweathering conditions and provenance. Geology,1995:23(10):921–924.
18. Floyd PA, Leveridge BE. Tectonic environment of the Devonian Gramscatho basin, south Cornwall: framework mode and geochemical evidence from turbiditic sandstones. J Geol Soc Lond,1987:144:531–42.
19. Garver JI, Royce PR, Smick TA. Chromium and nickel in shale of the taconic foreland; a case study for the provenance of fine-grained sediments with an ultramafic source. J Sedim Res,1996:66:100–106.
20. Guo Y, Li Y, Deng K, Wang Z, Yan S. Decoding the signals of sediment weathering: Toward a quantitative approach. Chemical Geology,2024:651:122009.
21. Hayashi KI, Fujisawa H, Holland HD, Ohmoto HY. Geochemistry of 1.9 Ga sedimentary rocks from Northeastern Labrador. Canada Geochem Cosmochim Acta,1998:61:4115–4137.
22. ICS. International Commission on Stratigraphy. International Chronostratigraphic Chart. IUGS-ICS, 2024.
23. Jones B, Manning DC. Comparison of geochemical indices used for the interpretation of paleo-redox conditions in ancient mudstones. Chem Geol,1994:111:111–129.
24. Kato Y, Fujinaga K, Nakamura K, Takaya Y, Kitamura K, Ohta J, et al. Deep-sea mud in the Pacific Ocean as a potential resource for rare-earth elements. Nature Geoscience,2011:4(8):535–539.
25. Liu G, Zhou DS. Application of micro elements analysis in identifying sedimentary environment. Exp Pet Geol,2007:29:307–314.
26. Louis P. Contribution géophysique à la connaissance géologique du bassin du lac
27. Tchad. Mémoire ORSTOM, 1970, 42.
28. Madhavaraju J, Loser H, Lee YI, Lozano-Santacruz R, Pi-Puig T. Geochemistry of Lower Cretaceous limestones of the Alisitos Formation, Baja California, Mexico: implications for REE source and paleo-redox conditions. J Sth Am Earth Sci,2016:66:149–165.
29. McDonough WF, Sun S. The Composition of the Earth. Chemical Geology,1995:120:223–253.
30. McLennan SM. Weathering and global denudation. The Journal of Geology,1993:101(2):295–303.
31. McLennan SM, Hemming S, McDaniel DK, Hanson GN. Geochemical Approaches to Sedimentation, Provenance and Tectonics. In: Johnsson, M.J. and Basu, A., Eds., Processes Controlling the Composition of Clastic Sediments, Geological Society of America, Special Papers,1993:285:21-40.
32. Moussa A. Les séries sédimentaires fluviatiles, lacustres et éoliennes du bassin du Tchad depuis le Miocène terminal. PhD thesis, Université de Strasbourg, 2010.
33. Nesbitt HW, Young GM. Early Proterozoic climates and plate motions inferred from major element chemistry of lutites. Nature,1982:299(5885):715–717.
34. Nesbitt HW, Young GM. Prediction of some weathering trends of plutonic and volcanic rocks based on thermodynamic and kinetic considerations. Geochimica et Cosmochimica Acta,1984:48(7):1523–1534.
35. Pias J. Quatre deltas successifs du Chari au quaternaire (République du Tchad et du Cameroun). C.R. Acad. Sci. (Paris), D,1967:264:2357–2360.
36. Pourmand A, Dauphas N, Ireland TJ. A novel extraction chromatography and MC-ICP-MS technique for rapid analysis of REE, Sc and Y: Revising CI-chondrite and Post-Archean Australian Shale (PAAS) abundances. Chemical Geology,2012:291:38–54.
37. Rimmer SM. Geochemical paleoredox indicators in Devonian- Mississippian black shales, Central Appalachian Basin (USA). Chem Geol,2004:206:373–391.
38. Roser BP, Korsch RJ. Provenance signatures of sandstone mudstone suites determined using discriminant function analysis of major element data. Chem Geol,1988:67:119–139.
39. Roy DK, Roser BP. Climatic control on the composition of Carboniferous–Permian Gondwana sediments, Khalaspir basin, Bangladesh. Gondwana Research,2013:23(3):1163–71.
40. Rudnick RL, Gao S. Composition of the Continental Crust. In: Holland HD and Turekian KK, Eds, Treatise on Geochemistry, Elsevier, Oxford, 2014, 1–51.
41. Servant M, Servant-Vildary S. L'environnement quaternaire du bassin du Tchad. In : Williams MAJ, Faure H, éd. : The Sahara and the Nile. Quaternary Environments and prehistoric occupation in northern Africa, Balkema, Rotterdam, The Netherlands, 1980, 113–162.
42. Shaltami O, Ben Hkoma M. Assessing Paleoclimate through Major and Trace Element Concentrations: A Review. Alq J Med App Sci,2024:7(4):1187–1193.
43. Singh P. Major, trace and REE geochemistry of the Ganga River sediments: Influence of provenance and sedimentary processes. Chemical Geology,2009:266(3–4):242–255.
44. Song MS. Sedimentary environment geochemistry in the Shasi section of Southern Ramp, Donying depression. J. Mineral. Petrol,2005:25:67–73.

45. Taylor SR, McLennan SM. The Continental Crust: Its Composition and Evolution. Blackwell, 1985.
46. Togozo FT, Boboye OA, Tchouatcha MS, Toyama R, Adeleye M, Babai AMA, et al. Geochemical constraints on provenance history, tectonic setting, and hydrocarbon generation potential of detrital deposits from the Carnot Berberati Basin, Southwest Central African Republic. Discov Geosci,2025:3:206.
47. Toteu SF, Penaye J, Poudjom Djomani YH. Geodynamic evolution of the Pan-African belt in Central Africa with special reference to Cameroon. Canadian Journal of Earth Sciences,2004:41:73–85.
48. Toteu SF, de Wit M, Pénaye J, Drost K, Alice Tait J, Houketchang Bouyo M, et al. Geochronology and correlations in the Central African Fold Belt along the northern edge of the Congo Craton: new insights from U-Pb dating of zircons from Cameroon, Central African Republic, and south-western Chad. Gondwana Res,2022:107:296–324.
49. Tribovillard N, Algeo TJ, Lyons T, Riboulleau A. Trace metals as paleo-redox and paleo-productivity proxies: an update. Chem Geol,2006:232:12–32.
50. Verma SP, Armstrong-Altrin JS. New multi-dimensional diagrams for tectonic discrimination of siliciclastic sediments and their application to Precambrian basins. Chemical Geology,2013:355:117–133.
51. Verma SP, Armstrong-Altrin JS. Geochemical discrimination of siliciclastic sediments from active and passive margin settings. Sedimentary Geology,2016:332:1–12.
52. Wana K, Taisso MH, Andossa L, Djetenbe B. Evaluation of the Level of Pollution by Heavy Metals of Market Garden Soils along the Chari River in Ndjamena: Case of the 9th and 7th Districts. Agricultural Sciences,2024:15:939-961.
53. Xie Y, Hou Z, Goldfarb RJ, Guo X, Wang L. Rare earth element deposits in China. In P. L. Verplanck & M. W. Hitzman (Eds.), Rare Earth and Critical Elements in Ore Deposits, Society of Economic Geologists,2016:18:115–136.
54. Xie G, Shen Y, Liu S, Hao W. Trace and rare earth element (REE) characteristics of mudstones from Eocene pinghu formation and Oligocene Huagang formation in Xihu Sag, East China sea basin: implications for provenance, depositional conditions and paleoclimate, Mar. Petrol. Geol,2018:1:1-35.
55. Xu QL, Liu B, Ma YS, Song XM, Wang YJ, Chen ZX. Geological and geochemical characterization of lacustrine shale: A case study of the Jurassic Da'anzhai member shale in the central Sichuan Basin, southwest China. J. Nat. Gas Sci. Eng,2017:47:124-139.
56. Xu DX, Cheng XP, Huang CL, Liu XR, Xie CD, Qiu RL, et al. Recovery of rare earth elements from sediments affected by mining activities. Journal of Hazardous Materials,2025:496:139223.
57. Yika LP, Djibril KNG, Afahnwie NA, Wochoko P, Mufur AM, Tita Awah MT, et al. Rare earth element geochemistry and resource potential of alluvial sediments from the Mugheb watershed, Cameroon volcanic line. Discov Geosci,2026:4:195.
58. Zou C, Mao L, Tan Z, Zhou L, Liu L. Geochemistry of major and trace elements in sediments from the Lubei Plain, China: Constraints for paleoclimate, paleosalinity, and paleoredox environment. Journal of Asian Earth Sciences: X,2021:6:100071.